JOURNAL OF PROPULSION AND POWER
Vol. 12, No. 5, September–October 1996

Condensed-Phase Kinetics of Cyclotrimethylenetrinitramine by Modeling the T-Jump/Infrared Spectroscopy Experiment

Stefan T. Thynell*
Pennsylvania State University, University Park, Pennsylvania 16802
and
Polly E. Gongwer† and Thomas B. Brill‡
University of Delaware, Newark, Delaware 19716

During the combustion of solid propellants, explosives, or pyrotechnics, the condensed phase experiences heating rates that may exceed 20,000 K/s. At such high heating rates, the thermal decomposition behavior of the energetic material could be affected by its rate of decomposition. To simulate the high heating rate environment, the T-jump experiment was developed for use with Fourier-transform infrared spectroscopy. The T-jump experiment utilizes electrical resistance heating of a thin Pt filament on which a small amount of the energetic test sample is placed. This work describes a heat transfer model of the filament and sample, a model of the current's control circuit, and global decomposition and heat release mechanisms of cyclotrimethylenetrinitramine (RDX), which is an energetic ingredient used in propellants and explosives. Comparisons of model calculations with experimental data reveal an excellent agreement. Similarly, the predicted time to rapid heat release for the highly energetic RDX sample also shows a good agreement with experimental results. Thus the use of the developed model in conjunction with experiments should be a useful tool in studying the thermal decomposition behavior of energetic materials under combustion-like conditions.

Nomenclature

A = pre-exponential factor
A_f = cross-sectional area of filament
c, c_p = specific heat
E = activation energy
g_1, g_2 = gains of electronic circuit
h = heat transfer coefficient
h_g = enthalpy of gas
i = current
k = thermal conductivity
L_s = length of sample
m = mass
N = number of species
Nu_w = Nusselt number
q = heat transfer
Ra = Rayleigh number
R_u = universal gas constant
T = temperature
t = time
t_{c1}, t_{c2} = time constants of electronic circuit
u = internal energy
V = voltage drop across filament
w = width of filament
x = axial coordinate
Y = species mass fraction
α = thermal diffusivity or coefficient of electrical resistivity
β = thermal expansion coefficient
Δh_f^0 = heat of formation
ε = emissivity
ν = kinematic viscosity
ρ_e = resistivity of filament
ρ_f = density of filament
ρ_s = density of sample
σ = Stefan–Boltzmann constant
$\dot{\omega}_i'''$ = species production

Subscripts
av = average
cond = conduction
conv = convection
e = electrical
ex = time to explosion
f = filament
g = gas
i = ith species
in = initial
l = liquid
lg = liquid to gas
max = maximum
rad = radiation
ref = reference quantity
s = sample
set = set or prescribed condition
sur = surroundings
0 = sample location

Superscripts
′ = per unit length
± = left (−) or right (+) side at $x = L_s$

Received Feb. 23, 1995; revision received April 3, 1996; accepted for publication April 8, 1996.

*Associate Professor, Department of Mechanical Engineering. Member AIAA.
†Graduate Research Assistant, Department of Chemistry and Biochemistry.
‡Professor of Chemistry, Department of Chemistry and Biochemistry.

Introduction

HEATING rates on the order of 20,000 K/s or higher are common in a wide variety of applications. During the combustion of solid propellants, explosives, or pyrotechnics, the condensed phase may regress at rates over 0.1 m/s. The conversion of the condensed phase into a gas phase occurs in a thin zone near the burning surface, and the thickness of this

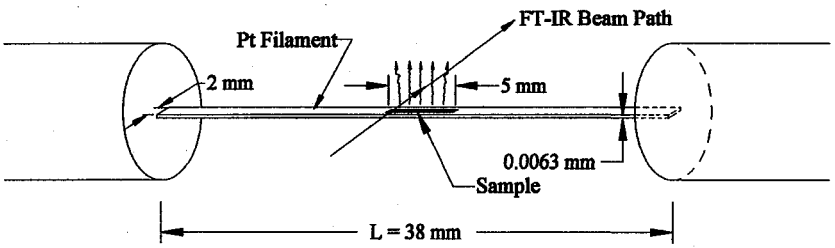

Fig. 1 Schematic diagram of filament dimensions and sample location.

zone is much smaller than 1 mm. In laser processing applications, such as cutting of ceramics, the heating rates are also high and thermal decomposition of the material may occur. To improve our understanding of the important pathways describing the material's thermal decomposition and subsequent chemical reactions, novel experimental techniques are needed that simulate the high heating rate environment.

There are numerous studies available in the literature that were focused on the thermal decomposition and combustion behavior of energetic materials, such as solid propellants or explosives. Most of the experimental studies utilized burners in which a small propellant strand was burnt in a steady-state fashion. A wide variety of nonintrusive techniques were utilized to study the flame zone including, among others, planar laser-induced fluorescence,[1] coherent anti-Stokes Raman spectroscopy,[2] UV/visible,[3] and Fourier-transform infrared (FTIR) spectroscopy.[4,5] The use of these techniques yielded important information on the overall flame structure of the energetic material. However, the success of probing in a region covering a distance of about 1–50 μm near the burning surface was limited because of difficulties associated with low signal-to-noise ratio (SNR), irregular geometrical surface structure, high burn rates of the energetic material, and required high operating pressures of the inert gas within the strand burner. As a result, the development of other experimental approaches for studying the thermal decomposition behavior of energetic materials continues to be of utmost importance.

One such alternative approach involves rapid heating of a plate or ribbon on which a small amount of the test sample is placed. In the fast thermolysis experiment,[6] a nichrome plate is heated electrically at specified rates. However, it is difficult to control the heating rate and to control the heating to a set temperature, while measuring changes in the resistance of the ribbon. Changes in the resistance are related to the endothermicity or exothermicity of the decomposition event and are important to monitor. By measuring the composition of the evolved gas-phase species, it is possible to learn much about the compositional changes that occur within the condensed phase. As an alternative method to the use of a nichrome ribbon, the T-jump experiment was developed.[7] This experiment utilizes a thin Pt filament, rather than a nichrome ribbon, to achieve high heating rates while recording the endothermicity or exothermicity of the decomposition process. The heating rates and set temperature are controlled by a sophisticated control circuit.

The objective of this work is to extend the previous heat transfer model of the filament,[7] to summarize the control circuit for the current flow in the filament and its model, to include a representative chemical kinetic scheme of cyclotrimethylenetrinitramine (RDX), and to compare results from model calculations with results obtained in experiments. The extension of the model includes the following: 1) lumped treatment of sample mass with filament over the contact area, 2) a model for the instantaneous change of current, and 3) the account for finite rate chemical kinetics.

Description of T-Jump Experiment

A schematic view of the Pt filament and its holders, sample size and its placement is shown in Fig. 1. The length of the filament is 38 mm, its width is 2 mm, and its thickness is only 6.3 μm. The sample is placed in the middle of the filament along a notched groove, and typically only a sample mass of about 200 μg is needed to conduct the decomposition study. The ends of the filament are welded onto an electrically and thermally, highly conducting material. The filament assembly is enclosed in a well-sealed chamber that can be pressurized to 6.7 MPa (1000 psi) using an inert gas such as Ar, Xe, or He. The chamber has optical access to the modulated beam of an FTIR spectrometer through two ZnSe windows. The rapid-scanning FTIR spectrometer (Nicolet 20SXC and 800) allows for the detection of IR-active species evolving from the sample during its decomposition. The chamber fits inside the slightly expanded sample compartment of the FTIR spectrometer. During a typical experiment, the rapid-scanning spectrometer acquires data at the rate of 0.1 s/scan at 4-cm^{-1} spectral resolution covering wave numbers from 600 to 5000 cm^{-1} using a mercury–cadmium–telluride detector. The spectral absorbance data are quantified in terms of mole percent concentrations.

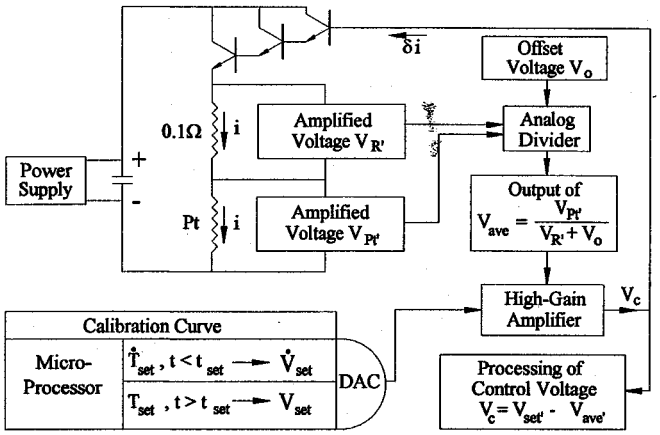

Fig. 2 Schematic diagram of circuit controlling current flow in the Pt filament.

The details of the electrical control circuit of the filament have been described,[7] and only a brief summary is presented here. Figure 2 shows a schematic diagram of the circuit controlling the flow of current through the Pt filament. The initial rapid temperature rise in the filament is caused by discharge from a row of capacitors. Simultaneously, the microprocessor rapidly increases the set-voltage input to the amplifier over a specified period of time, which depends on primarily the filament size. Subsequently, the microprocessor outputs a constant set voltage, which allows the filament to reach a steady-state temperature. Typically, a steady-state condition is reached within 0.4 s at a heating rate of 2000 C/s. During an exothermic or endothermic event of the energetic sample, the filament resistance changes, which causes a change in the voltage V_{av}. The acquisition of data on the control voltage V_c is performed by utilizing a standard personal computer.

Model Assumptions

To simulate the thermal response of and current flow through the filament, as well as the thermal decomposition and

heat release processes within the sample, the following set of assumptions is introduced.

1) The sample and filament remain in excellent contact throughout the heating event. As a result, the temperature difference between the sample and filament is negligibly small over the contact area. The sample is typically either small crystals having an average diameter of 10 μm or less, or it is a very fine powder.

2) The temperature of the filament varies with time and a coordinate axis aligned between the two filament holders.

3) The thermal inertia of the two filament holders is large, allowing the assumption of constant temperature at the two ends of the filament.

4) The specific heat and thermal conductivity of the Pt filament are independent of temperature.

5) Because of the lack of availability of appropriate correlation for transient natural convection heat transfer from the thin filament covering the low Rayleigh range (5–20), it is assumed that a correlation describing convective heat transfer from a horizontal cylinder is applicable.

6) The emissivity of the filament is independent of wavelength and temperature, and the filament area is small compared to the area of the surroundings.

7) The mass-loss rate via gasification of the sample is known from separate experiments.

8) Possible heat release from gasified products does not affect processes occurring within the sample. Mixing with the surrounding inert gas should effectively quench any such reactions.

9) Melting of the sample occurs at a known temperature; at the melting point, a negligible amount of thermal decomposition has occurred.

10) A first-order, linear control system describes the rate of change of the current flow through the filament.

Further discussion of the first and fifth assumptions is warranted. The filament is typically cupped rather than kept flat to obtain a filament with a certain degree of stiffness. That is, the geometry of the filament's cross section is similar to a sector of an annulus rather than a rectangle. This geometrical change has a strong influence on the gas-phase temperature in close vicinity of the sample: the thermal boundary layer rapidly surrounds the sample to cause a small temperature difference between the sample and filament. The cupping also allows one to use a heat transfer correlation of a horizontal cylinder.

Model Description

Conservation of Sample Mass and Energy

A schematic view of the control volumes used to develop the physical model is illustrated in Fig. 3. The temperature varies with time and along the axial coordinate, whose origin is placed at the center of the filament. Transient, one-dimensional heat conduction occurs within the filament. Heat losses occur by convection and radiation along the surface of the filament, as well as during the mass loss via gasification from the sample. Conservation of sample mass, conservation of energy of sample and filament over the distance in which they are in direct contact, and conservation of energy of filament in regions away from the sample yield the following expressions:

$$\frac{\mathrm{d}m_s}{\mathrm{d}t} = -m_s A_{\mathrm{lg}} \exp\left(-\frac{E_{\mathrm{lg}}}{R_u T_0}\right) \tag{1}$$

$$\frac{\partial}{\partial t}(m_{f,0} c_f T_0 + m_s u_s) = -2(q_{\mathrm{cond}} + q'_{\mathrm{conv}} L_s + q'_{\mathrm{rad}} L_s) + i^2 \rho_{e,0} \frac{L_s}{A_f} + \dot{m}_s h_g, \qquad 0 < x < \frac{L_s}{2} \tag{2}$$

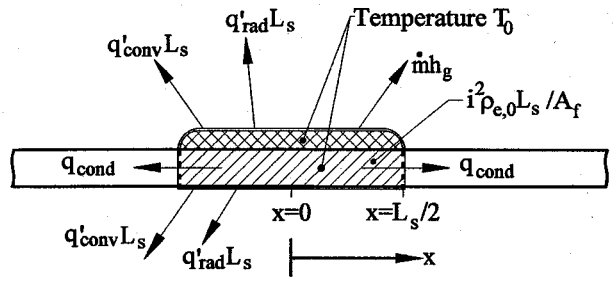

Fig. 3 Control volume and energy fluxes associated with sample and filament.

$$\rho_f c_f A_f \frac{\partial T}{\partial t} = k_f A_f \frac{\partial^2 T}{\partial x^2} - 2(q'_{\mathrm{conv}} + q'_{\mathrm{rad}}) + i^2 \frac{\rho_e}{A_f} \qquad \frac{L_s}{2} < x < \frac{L}{2} \tag{3}$$

The initial and boundary conditions of the previous set of equations are as follows:

$$m_s = m_{s,\mathrm{in}}, \qquad t = 0 \tag{4a}$$

$$T(x, t) = T_{\mathrm{in}} = T\left(\frac{L}{2}\right), \qquad 0 \le x \le \frac{L}{2}, \qquad t = 0 \tag{4b}$$

$$\frac{\partial T}{\partial x} = 0, \qquad x = 0, \qquad t > 0 \tag{4c}$$

$$T\left(\frac{L_s^-}{2}, t\right) = T\left(\frac{L_s^+}{2}, t\right), \qquad x = \frac{L_s}{2}, \qquad t > 0 \tag{4d}$$

$$k_f \left.\frac{\partial T}{\partial x}\right|_{x=L_s^-/2} = k_f \left.\frac{\partial T}{\partial x}\right|_{x=L_s^+/2} \tag{4e}$$

Evaluation of internal energy of sample u_s, enthalpy of gas leaving sample h_g, and heat losses by conduction, convection, and radiation are, respectively, determined from

$$u_s = \sum_{i=1}^{N} Y_i [c_{s,i}(T_0 - T_{\mathrm{ref}}) + \Delta h^0_{f,s,i}] \tag{5a}$$

$$h_g = \sum_{i=1}^{N} Y_i [c_{\mathrm{pg},i}(T_0 - T_{\mathrm{ref}}) + \Delta h^0_{f,g,i}] \tag{5b}$$

$$q_{\mathrm{cond}} = -k_f A_f \frac{\partial T}{\partial x} \tag{5c}$$

$$q'_{\mathrm{conv}} = hw(T - T_g) \tag{5d}$$

$$q'_{\mathrm{rad}} = \varepsilon \sigma w (T^4 - T^4_{\mathrm{sur}}) \tag{5e}$$

$$\rho_e = \rho_{e,\mathrm{ref}}[1 + \alpha(T - 273.15)] \tag{5f}$$

The correlation used to calculate the convective heat transfer coefficient is given by

$$Nu_w = hw/k_g = 1.02 Ra^{0.148} \tag{6}$$

where the Rayleigh number is defined as

$$Ra = \frac{g\beta(T - T_g)w^3}{\nu_g \alpha_g} \tag{7}$$

In Eqs. (5d), (6), and (7), an effective diameter rather than width is used ($w = \pi d$) as discussed previously. For most gases and pressures of interest, the Rayleigh number varies from 1 to 20. The average temperature of the filament T_{av} is computed from

$$T_{av} = \frac{1}{L}\int_0^L T(x, t)\, dx \tag{8}$$

Model of Current Flow

The circuit controlling the current flow through the filament is treated as a first-order, linear system.[8] The expressions governing current flow are specified by

$$\frac{di}{dt} = -\frac{i}{t_{c1}} + g_1\left(\left.\frac{dT_{av}}{dt}\right|_{set} - \frac{dT_{av}}{dt}\right) \tag{9a}$$

$$\frac{di}{dt} = -\frac{i}{t_{c2}} + g_2(T_{set} - T_{av}) \tag{9b}$$

where t_{c1} and t_{c2} are the time constants of the controller response, and g_1 and g_2 are the gain factors. The set rate of change of temperature $dT_{av}/dt|_{set}$ and set temperature T_{set} are specified, whereas the time constants and gains were determined from separate measurements. The first expression for the current is used during the ramping of the temperature. Once the average temperature within filament is within 25 K of the set temperature, the second expression is used to calculate the current. It is also observed that at steady-state conditions, the average temperature never approaches the set temperature. Such a situation would require a zero current flow in the previous model. Thus the current flow through the filament approaches $0.1(T_{set} - T_{av})$ near steady state, because the experimentally determined values of the time constant and gain are, respectively, $t_{c2} = 0.01$ s and $g_2 = 10$ A/K − s.

Global Reaction Mechanism of RDX and Species Conservation

A considerable amount of work has been performed to determine the relevant thermal decomposition pathways of RDX.[9-12] In spite of such efforts, much more work needs to be performed to determine the rate constants for its major decomposition pathways. As a result, it is assumed that the following mechanism can be used to describe RDX decomposition:

$$RDX \rightarrow 3CH_2O + 3N_2O \tag{10}$$

$$RDX \rightarrow 3NO_2 + 3H_2CN \tag{11}$$

Here, reaction (10) is favored at lower temperatures and is exothermic. Reaction (11) is endothermic and is favored at higher temperatures. Both of these reactions are treated as first-order, unimolecular decomposition reactions. The major heat release among the pyrolysis products is thought to occur from a reaction between the formaldehyde (CH_2O) and nitrogen dioxide (NO_2) given by

$$CH_2O + NO_2 \rightarrow CO + NO + H_2O \tag{12}$$

In this work, the reaction (12) is assumed to take place primarily in the liquid phase, and is treated as a second-order reaction occurring within the liquid phase, whose density is used to compute the molar concentration. As a result, the rate constants deduced by Lin et al.[13] in shock-tube studies may not be directly applicable. The products formed according to these reactions are considered to be dissolved gases in the RDX liquid phase. The rate constants for the previous reactions are expressed in a usual Arrhenius form, namely,

$$k = AT^a \exp(-E/R_u T) \tag{13}$$

The application of the previous three-step reaction mechanism assumes that reactions only proceed in the forward direction. It is highly unlikely that significant recombination among the products from any one of the above reactions occurs. The species conservation expression is given by

$$\frac{dY_i}{dt} = \frac{\dot{\omega}_i'''}{\rho_s}, \qquad i = 1, \ldots, N \tag{14a}$$

$$\sum_{i=1}^{N} Y_i = 1 \tag{14b}$$

Here, the net rate of species production $\dot{\omega}_i'''$ is computed according to available expression.[14]

Method of Solution

The previous problem involves both a solution to a partial differential equation (PDE) and to a set of coupled (ODEs) for overall mass and species conservation. In this work, the spatial derivatives appearing in the PDEs for temperature were discretized utilizing a stretched grid. As a result, a system of coupled ODEs was obtained and numerically integrated in time. The system of equations is highly stiff, but the routine STIFBS developed by Press et al.[15] experienced no difficulty in integrating the system of differential equations. A total of 48 unknowns was involved, including 40 temperatures, 7 species and sample mass. During the melting of RDX, enthalpy replaced the center temperature as the dependent variable in the energy equation.

Discussion of Results

In this section, the results from a study using the previously described model for thermal decomposition and reaction of RDX, as well as comparison with data acquired from experiments will be discussed. Focus of such a discussion will first be made on the thermal response of the filament and then on the predicted chemical kinetics behavior of RDX, including species evolution, heat release, and time to rapid heat release. It is in this latter portion that the modeling results will be compared with experimental results.

Table 1 shows the values of A and E that have been assumed in this study. As will be discussed later, changes to the values of the pre-exponential factor and activation energy were required from the baseline case to reach an agreement with the experimental data. The results shown in Figs. 4–7 were obtained using the chemical kinetic data of Set 1 and input properties from Brill et al.[7] In addition, thermodynamic properties were evaluated from a database compiled by Kee et al.,[16] and the liquid-to-gas conversion rate was computed using $A_{lg} = 1.98 \times 10^{14}$ (1/s) and $E_{lg} = 38.2$ kcal/mol.[17]

Figures 4 and 5 show, respectively, the spatial variation of the filament temperature at four specific time intervals and the temporal variation of the average and the centerline temperature. The Pt filament was surrounded by an argon gas at a total pressure of 4 atm. Inspection of these figures reveals the following. First, the rapid rate of change of the current flow via Eq. (9a) causes the average temperature to reach a constant value in a short period of time (see Fig. 5). However, although the average temperature reaches a steady value within about 0.2 s, the center temperature has not reached a steady-state value within this time period. The 200 μg of energetic sample causes a significant time delay, and more than 1 s would be required to reach a steady-state value of the center temperature. There appears to be at least two options to reduce the time to

Table 1 Definition of rate constants for reaction sets employed in model calculations

	$RDX \rightarrow 3CH_2O + 3N_2O$		$RDX \rightarrow 3NO_2 + 3H_2CN$		$NO_2 + CH_2O \rightarrow CO + NO + H_2O$	
Set number	*A*, 1/s	*E*, kcal/mol	*A*, 1/s	*E*, kcal/mol	*A*, cm^3/mol-s	*E*, kcal/mol
1	4×10^{13}	36	16×10^{16}	45	$802 \times T^{2.77}$	25.73
2	0.794×10^{13}	34.4	2.51×10^{16}	44.1	$8.69 \times T^{2.77}$	17.85
3	6×10^{13}	36	16×10^{16}	45	$802 \times T^{2.77}$	25.73
Baseline	1×10^{13}	36	2×10^{16}	45	$802 \times T^{2.77}$	13.73

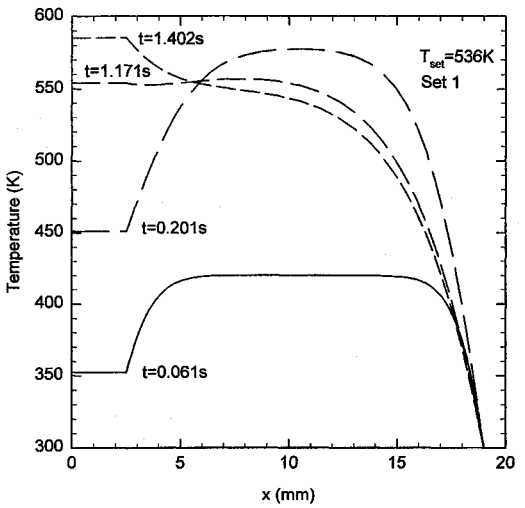

Fig. 4 Spatial variation of filament temperature at four selected time intervals.

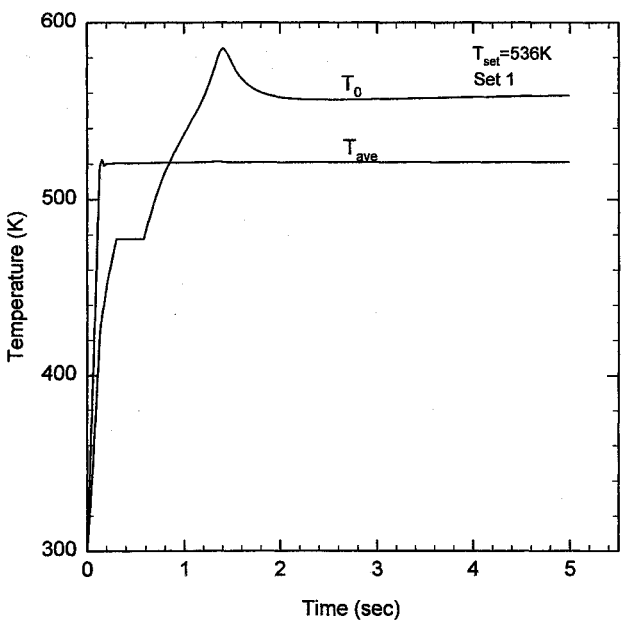

Fig. 5 Temporal change of center and average temperature of Pt filament.

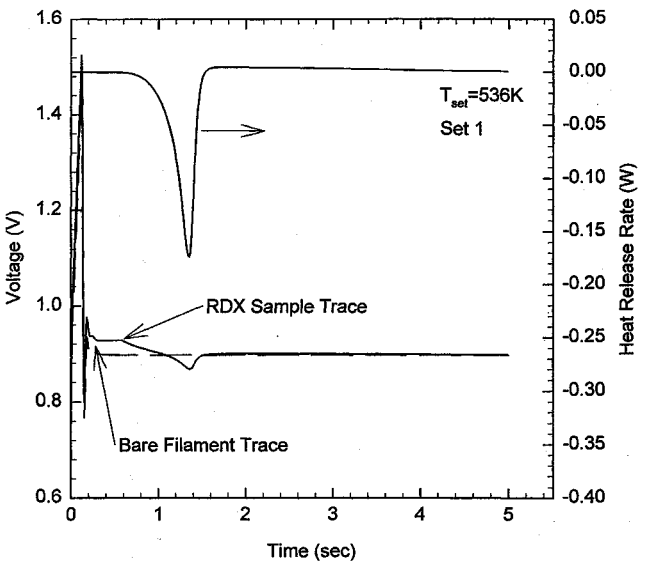

Fig. 6 Voltage drop across Pt filament with and without sample and heat release rate from chemical reactions.

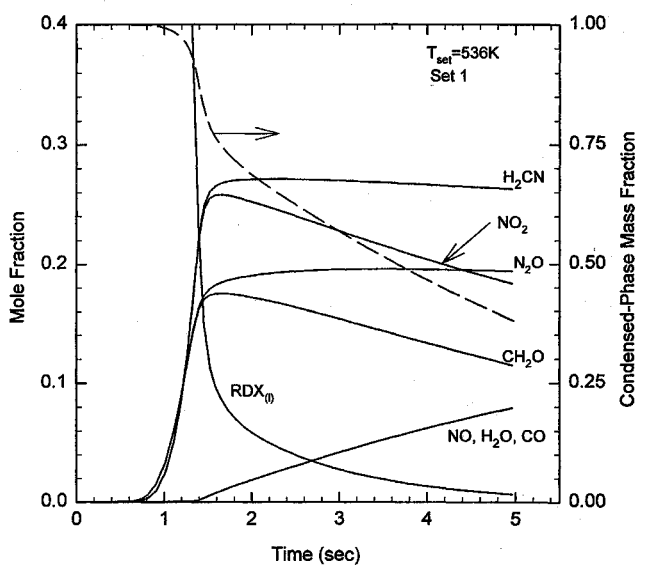

Fig. 7 Temporal evolution of species mole fractions and condensed-phase mass fraction remaining.

reach a steady-state value. On the one hand, the sample mass could be reduced, but the detectability of the evolved gases (SNR) controls the lower limit that can be used. On the other hand, it is possible to use a Pt filament that has a larger cross-sectional area to allow a larger rate of energy generation from the flow of current. A larger cross-sectional area (increase of its thickness) would also increase conductive heat transfer into the sample position region and establish a more uniform temperature in the filament over the distance from $x = 0$ to $x = 10$ mm. A thicker filament would, however, decrease the sensitivity to changes in the heat release rate of the sample, as well as increase conductive heat transfer into the filament holder. Furthermore, it could also be difficult to maintain the filament holder at a prescribed temperature. In practice, events shorter than 1 s are rarely discussed in T-jump/FTIR spectroscopy determinations of the chemistry.[7]

Second, melting and heat release processes from chemical reactions within the sample are clearly revealed. Melting occurs at 478 K and lasts about 0.3 s, as shown in Fig. 5. The exothermic event triggered by heat release from reaction (12)

commences at about $t = 1.4$ s. A peak temperature of about 585 K or about a temperature rise of about 30 K is associated with a net exothermicity of reactions (10–12).

Finally, the change in the average temperature associated with the endothermic and exothermic events is barely noticeable in Fig. 5. However, the data acquisition system, which records an amplified difference between the set voltage and voltage drop across the Pt filament (V_c in Fig. 2), has no difficulty in recording both endothermic events associated with melting of the sample and the endothermic and exothermic events associated with the sample.[7]

Figure 6 depicts the voltage drop across the filament with and without the sample, as well as the heat release rate associated with reactions (10–12) and evaporation of $RDX_{(l)}$. The voltage drop across the filament changes in an oscillatory fashion during the first 0.2 s of the event because of a change in the sign of the term in the right-hand side of Eq. (9c). It should be noted that this oscillatory behavior is also observed experimentally in the measured control voltage. During decomposition and subsequent chemical reactions among products, the control circuit responds and attempts to maintain the average temperature constant and at a level slightly below the set value. The initiation of the heat release (negative value implies exothermicity) at $t = 0.7$ s is caused by reaction (10). However, endothermicity because of reaction (11) and evaporation produce a net decrease in heat release, although reaction (12) starts to play an important role. With rapid depletion of $RDX_{(l)}$, the heat release rate stays slightly positive because of a balance between evaporation (endothermic) of $RDX_{(l)}$, and net exothermicity of reactions (10–12).

Figure 7 shows the evolution of species mole fraction and the condensed-phase mass fraction remaining. The decomposition commences at about $t = 0.70$ s and reaches a peak at $t = 1.4$ s, corresponding to the time of maximum sample temperature. At the time of peak temperature, reaction (12) begins and depletes the concentration of CH_2O and NO_2. Since the rate of evaporation is species independent, changes in concentration of H_2CN and N_2O are caused by the relative importance in the decomposition pathway of reactions (10) and (11). At this temperature and chosen set of rate constants, the thermal decomposition of $RDX_{(l)}$ favors reaction (11) over reaction (10). Near the time $t = 5$ s, a condensed-phase residue remains on the filament, and this is also observed experimentally; however, the specific chemical composition of the residue is not known.

The last set of results is focused on an attempt to duplicate the measured time-to-explosion data of RDX vs the set temperature of the filament in an Ar environment at 4 atm. Time-to-explosion refers to time of peak heat release, which in Fig. 6 occurred at $t = 1.4$ s. To obtain a reasonable agreement with the experimental results shown in Fig. 8, the baseline set of pre-exponential factors and activation energies required modification. For example, the use of $E = 13.73$ kcal/mol for reaction (12) produces a complete consumption of CH_2O. Since CH_2O is observed in the gas-phase region by FTIR spectroscopy, reaction (12) occurs too fast. It is believed that reaction (12) is too fast because the pre-exponential factor and activation energy were deduced from gas-phase measurements, whereas in this work these data were assumed to be applicable for the heterogeneous condensed phase. The use of either Set 1, 2, or 3 in Fig. 8 yields a reasonable agreement with the measured data. The expected behavior of t_{ex} should be further discussed. Figure 8 reveals the presence of three distinct regions, and a fourth one is expected to exist. The first region applies to $1/T_{max} > 1.88 \times 10^{-3}$, and it implies very slow, pure evaporation of the sample. The temperatures are too low to produce a sufficiently high concentration of CH_2O/NO_2 for rapid heat release. The second region covers $1.8 \times 10^{-3} < 1/T_{max} < 1.88 \times 10^{-3}$ and is dominated by the evaporation process. The third region spans $1.58 \times 10^{-3} < 1/T_{max} < 1.8 \times 10^{-3}$ and is controlled by chemical kinetic processes occurring within the sample. The fourth (expected) region has not been revealed experimentally, but it should demonstrate the presence of a minimum time-to-explosion $t_{ex,min}$ dictated by the finite rate chemical kinetics of RDX, and the finite amount of time it takes to raise the temperature of the Pt filament to its steady-state value. To establish this lower limit, faster heating of the sample is required than presently possible.

To ascertain which one of the three sets of rate constants of Table 1 that seems to best represent thermal decomposition and subsequent reaction of RDX, it is necessary to compare the modeling results with an additional set of data. Figure 9 shows the molar concentration ratio of N_2O/NO_2 obtained from measurements and modeling. The darkened circles of experiments show that the concentration ratio varies from about two at low maximum temperatures, revealing the importance of the low-temperature pathway of reaction (10). At higher maximum temperatures, the ratio decreases and is about 0.75 at a peak

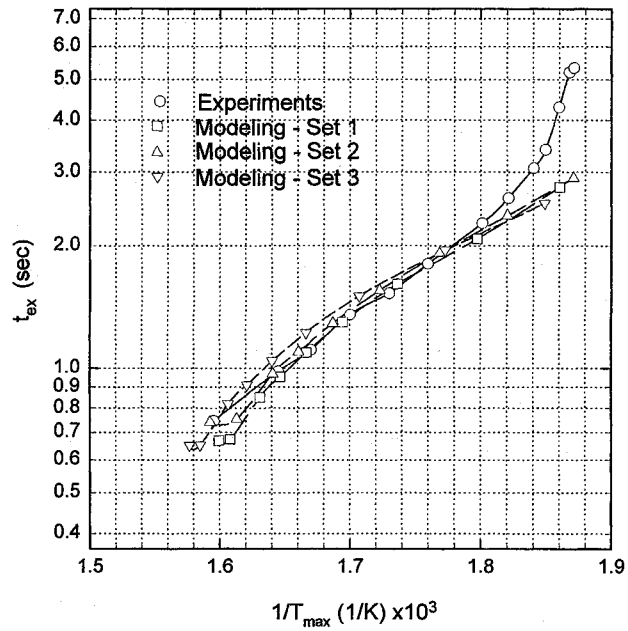

Fig. 8 Measured and predicted time-to-explosion vs maximum temperature.

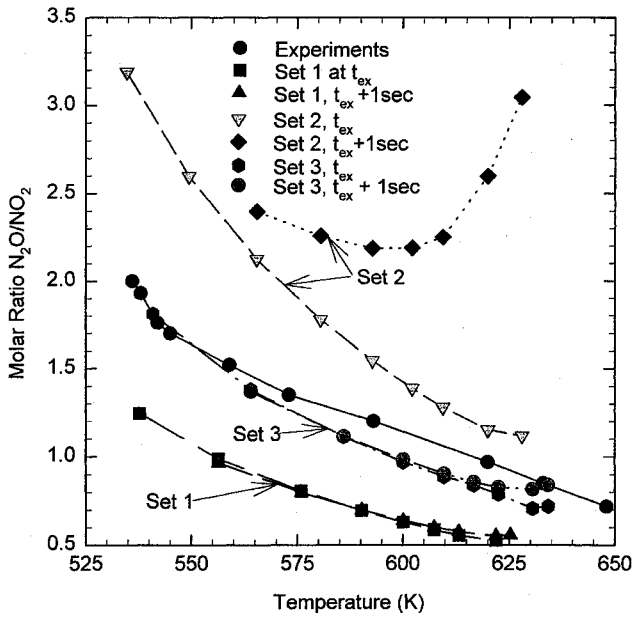

Fig. 9 Comparison of measured and predicted N_2O/NO_2 molar concentration ratios using chemical kinetic data in Table 1.

temperature of 630 K. From the modeling, molar concentration ratios of N_2O/NO_2 were computed at t_{ex} and 1 s beyond t_{ex}. Clearly, the rate constants from Set 3 seem to yield the best reproduction of the molar concentration ratio. The slight adjustment of A from 4×10^{13} in Set 1 to 6×10^{13} in Set 3 caused a marked improvement in the agreement with the experimental data. Since all three sets of kinetic data of Table 1 seem to yield a good agreement with experimental data of t_{ex}, the use of molar concentration ratio as a diagnostic tool is of utmost importance.

Summary and Conclusions

A comprehensive model of the T-jump experiment has been formulated and solved numerically. To compare the model results with experiments, a reduced chemical reaction mechanism of RDX involving a low- and a high-temperature decomposition pathway has been employed. A reaction mechanism involving CH_2O and NO_2 was assumed to predict the evolution of species from reaction among RDX decomposition products. Since chemical kinetic data for reactions occurring within a condensed phase are not well established, slight modifications to existing data were required to obtain reasonable agreement with experiment. Based on the three global reactions employed in this study, Set 3 of Table 1 produced the best agreement with experiments, both in terms of predicting the time at which maximum temperatures were established and the N_2O/NO_2 molar concentration ratios.

Acknowledgments

This work was performed under Contract DAAL03-92-G-0118 and supported by R. W. Shaw of the U.S. Army Research Office, Research Triangle Park, North Carolina.

References

[1]Parr, T., and Hanson-Parr, D., "Nonintrusive Diagnostic Techniques for Research on Nonsteady Burning of Solid Propellants," *Nonsteady Burning and Combustion Stability of Solid Propellants*, edited by L. DeLuca, E. W. Price, and M. Summerfield, Vol. 143, Progress in Astronautics and Aeronautics, AIAA, Washington, DC, 1992, pp. 261–324.

[2]Stufflebeam, J. H., Hall, R. J., and Verdieck, J. F., "CARS Diagnostics of High Pressure and Temperature Gases," *Combustion Diagnostics by Nonintrusive Methods*, edited by T. D. McCay and J. A. Roux, Vol. 92, Progress in Astronautics and Aeronautics, AIAA, New York, 1984, pp. 3–23.

[3]Vanderhoff, J. A., "Species Profiles in Solid Propellant Flames Using Absorption and Emission Spectroscopy," *Combustion and Flame*, Vol. 84, No. 1, 1991, pp. 73–92.

[4]Klotz, S., Thynell, S. T., Huang, I. T., and Kuo, K. K., "Analysis of Plumes of Solid Propellant Combustion Using an FT-IR Spectrometer," *Journal of Propulsion and Power*, Vol. 8, No. 3, 1992, pp. 537, 538.

[5]Mallery, C., Kim, E., and Thynell, S. T., "FT-IR Absorption Spectrometry of Propellant Flames," *JANNAF Combustion Subcommittee Meeting*, Chemical Propulsion Information Agency, Publ. 606, Vol. II, Monterey, CA, 1993, pp. 307–318.

[6]Oyumi, Y., and Brill, T. B., "Thermal Decomposition of Energetic Materials 3. A High-Rate, In Situ, FTIR Study of the Thermolysis of RDX and HMX with Pressure and Heating Rates as Variables," *Combustion and Flame*, Vol. 62, No. 3, 1985, pp. 213–224.

[7]Brill, T. B., Brush, P. J., James, K. J., Shepherd, J. E., and Pfeiffer, K. J., "T-Jump/FT-IR Spectroscopy: A New Entry into the Rapid, Isothermal Pyrolysis Chemistry of Solids and Liquids," *Applied Spectroscopy*, Vol. 46, No. 6, 1992, pp. 900–911.

[8]Shepherd, J. E., and Brill, T. B., "Interpretation of Time-to-Explosion Tests," *Proceedings of the 10th International Detonation Symposium*, U.S. Naval Surface Warfare Center, White Oak, MD, 1993, pp. 849–855.

[9]Boggs, T. L., "The Thermal Behavior of Cyclotrimethylenetrinitramine (RDX) and Cyclotetramethylenetetranitramine (HMX)," *Fundamentals of Solid Propellant Combustion*, edited by K. K. Kuo and M. Summerfield, Vol. 90, Progress in Astronautics and Aeronautics, AIAA, New York, 1984, pp. 121–175.

[10]Adams, G. F., and Shaw, R. W., Jr., "Chemical Reactions in Energetic Materials," *Annual Review of Physical Chemistry*, Vol. 43, 1992, pp. 311–340.

[11]Brill, T. B., and Brush, P. J., "Condensed Phase Chemistry of Explosives and Propellants at High Temperature: HMX, RDX and BAMO," *Philosophical Transactions of the Royal Society of London*, Vol. 339, No. 1654, 1992, pp. 377–385.

[12]Behrens, R., and Bulusu, S, "Thermal Decomposition of Energetic Materials IV: Deuterium Isotope Effects and Isotopic Scrambling (H/D, $^{13}C/^{18}O$, $^{14}N/^{15}N$) in Condensed Phase Decomposition of 1,3,5-Trinitro-Hexahydro-s-Triazine (RDX)," *Journal of Physical Chemistry*, Vol. 96, No. 22, 1992, pp. 8891–8897.

[13]Lin, C.-Y., Wang, H.-T., Lin, M. C., and Melius, C. F., "A Shock Tube Study of the $CH_2O + NO_2$ Reaction at High Temperatures," *International Journal of Chemical Kinetics*, Vol. 22, No. 5, 1990, pp. 455–482.

[14]Kuo, K. K., *Principles of Combustion*, Wiley, New York, 1986, p. 209.

[15]Press, W. H., Teukolsky, S. A., Vetterling, W. T., and Flannery, B. P., *Numerical Recipes in Fortran*, 2nd ed., Cambridge Univ. Press, New York, 1992, p. 737.

[16]Kee, R. J., Rupley, F. M., and Miller, J. A., "The Chemkin Thermodynamic Data Base," Sandia, Rept. SAND87-8215B, Dec. 1990.

[17]Huang, T. H., Thynell, S. T., and Kuo, K. K., "Modeling of Partially Confined Hot Fragment Conductive Ignition," *25th Symposium (International) on Combustion*, The Combustion Inst., Pittsburgh, PA, 1994, pp. 1595–1601.